Published online 25 July 2012 Nucleic Acids Research, 2012, Vol. 40, No. 15 e119
doi:10.1093/nar/gks701

A benchmark for chromatin binding measurements in live cells

Davide Mazza[1,2], Alice Abernathy[1], Nicole Golob[1], Tatsuya Morisaki[1] and James G. McNally[1,*]

[1]Laboratory of Receptor Biology and Gene Expression, National Cancer Institute, National Institutes of Health, 20892, Bethesda, MD, USA and [2]Davide Mazza, Istituto Scientifico Ospedale San Raffaele, Centro di Imaging Sperimentale e Università Vita-Salute San Raffaele - 20132, Milano, Italy

Received January 21, 2012; Revised June 8, 2012; Accepted June 26, 2012

ABSTRACT

Live-cell measurement of protein binding to chromatin allows probing cellular biochemistry in physiological conditions, which are difficult to mimic *in vitro*. However, different studies have yielded widely discrepant predictions, and so it remains uncertain how to make the measurements accurately. To establish a benchmark we measured binding of the transcription factor p53 to chromatin by three approaches: fluorescence recovery after photobleaching (FRAP), fluorescence correlation spectroscopy (FCS) and single-molecule tracking (SMT). Using new procedures to analyze the SMT data and to guide the FRAP and FCS analysis, we show how all three approaches yield similar estimates for both the fraction of p53 molecules bound to chromatin (only about 20%) and the residence time of these bound molecules (~1.8 s). We also apply these procedures to mutants in p53 chromatin binding. Our results support the model that p53 locates specific sites by first binding at sequence-independent sites.

INTRODUCTION

Binding to chromatin can be measured in living cells by detecting the retardation of a fluorescently tagged protein as it interacts with this relatively immobile scaffold (1–4). In fluorescence recovery after photobleaching (FRAP), the retardation is measured by performing a photobleach and then determining the rate of fluorescence entry into the bleached region (5,6). In fluorescence correlation spectroscopy (FCS), the retardation is measured by recording the fluctuations in fluorescence intensity in a small diffraction-limited spot, which reflect the random movement of molecules into and out of the spot (7–9). In single-molecule tracking (SMT), the retardation is measured by tracking individual molecules and directly identifying bound molecules as those that stop moving (2,10,11).

Different live-cell binding studies using these techniques have yielded widely divergent estimates with no consensus. For example, estimates of the chromatin-bound fraction of transcription factors have ranged from 20 to 99%, leading to disparate predictions about regulatory-site occupancy (2,6,12,13). These discrepancies are not limited to bound fractions, as estimates for transcription-factor residence times on chromatin have ranged from 0.005 to 4.5 s (2,6,11,12). Similar problems arise in the analysis of polymerase binding in live cells where estimates of elongation rates vary from 0.5 to 100 kb/min (14–18), and completely opposite conclusions have been reached about whether polymerase assembly is efficient (16) or inefficient (15). Several studies have suggested that many of these discrepancies could reflect technical errors (19,6), since each of the approaches used to measure live cell binding has limitations. Resolving these discrepancies is critical because *in vivo* measurements are essential for determining how cellular reactions proceed in the complex milieu of the live cell.

A fundamental limitation of FRAP and FCS is that they only indirectly measure the retardation due to binding by recording changes in fluorescence intensity. Binding estimates are extracted by fitting the intensity data with kinetic models (1) that make different assumptions about the protein's diffusion and binding behavior. For example, the kinetic models applied to transcription factors have posited either: (i) two binding states reflecting sequence-specific and sequence-independent binding (13); (ii) one binding state reflecting either sequence-specific (20) or sequence-independent binding (6,12,21); or (iii) two diffusing states reflecting two different molecular complexes of the transcription factor (7,9,22).

*To whom correspondence should be addressed. Tel: +1 301 402 0209; Fax: +1 301 496 4951; Email: mcnallyj@mail.nih.gov
Present address:
Alice Abernathy, Institut d'Investigacions Biomèdiques August Pi i Sunyer (IDIBAPS), 08036, Barcelona, Spain.

Compounding this complexity, different FRAP and FCS kinetic models have also made different assumptions about the protein's diffusion, assuming that it is fast enough to be ignored (13), or slow enough to be incorporated into the kinetic model (6,12).

For SMT, binding estimates are in principle more direct since bound molecules can be visualized (2). However, accurately identifying which segments of a trajectory reflect binding is complicated by the fact that even a completely stationary molecule will appear to move due to the precision limit of localization and a freely diffusing molecule will appear to be bound transiently if it undergoes a few small displacements.

Therefore, different strategies have been developed to discriminate between bound and free molecules in SMT (2,10,11). For example, bound molecules have been identified by setting two thresholds, an upper bound r_{max} for the maximum displacement of the molecule combined with a lower bound N_{min} for the minimum number of time points comprising a valid bound-molecule track (10,23). Once a classification is made, bound fractions are easily calculated based on the fraction of displacements that satisfy this classification, and residence times are estimated based on the duration of the selected displacements. However, identifying the best criteria to accurately identify bound molecules remains a key question in single molecule tracking.

In sum, while the techniques of FRAP, FCS and SMT are now well established, the analysis procedures applied to these data are not. As a result, a consensus on how to accurately measure live cell binding parameters is lacking, and this is a serious impediment to progress in understanding how binding reactions proceed within live cells.

Here we introduce two improved methods to quantify binding to intracellular scaffolds by SMT, and we also demonstrate how to achieve consensus with binding estimates obtained by FRAP and FCS. The first improvement in SMT is based on the objective selection of SMT tracks corresponding to bound molecules and the second improvement in SMT is based on kinetic modeling of the complete distribution of SMT displacements. After showing substantial agreement between these two SMT approaches for estimating live-cell binding for the tumor suppressor p53, we then show how the SMT data can also be used to select the most accurate kinetic model for FRAP and FCS. We demonstrate that upon application of our methods, FRAP, FCS and SMT yield very similar binding estimates, thereby establishing a consensus for live-cell binding measurements. Finally, to exemplify the relevance of such measurements, we discuss the binding analysis of p53 mutants by SMT, showing that p53 appears to locate target-sites by initial binding at sequence-independent sites followed by subsequent binding to specific target sites.

MATERIALS AND METHODS

Plasmid construction

The coding region of the wild-type p53, of the point-mutant p53-R273H, of the truncated p53-d30 (amino acids 1–363 of human p53) and of the double mutant p53-R273H/d30 were obtained by polymerase chain reaction (PCR) of either a p53-wt-GFP or a p53-R273H-GFP template, using the following primers: p53-F and p53-d30-F: 5′-GAC CGC GAT CGC CAT GGA GGA GCC GCA GTC AGA TCC TA-3′; p53-B: 5′-GTC GGT TTA AAC GTC TGA GTC AGG CCC TTC TGT CTT-3′; p53-d30-B: 5′-TGC GGT TTA AAC CCT GCT CCC CCC TGG CTC CTT CCC A-3′ and cloned into the C terminal HaloTag Flexi vector pFC15A (Promega Corp., Madison, WI, USA) by digesting the PCR product with SgfI and PmeI and the vector with SgfI and EcoICRI, and by subsequent ligation of the restriction products.

The coding region for histone H2B was obtained by PCR of an H2B-GFP template, using the following primers H2B-F: 5′-CTT GGC GAT CGC CAT GCC AGA GCC AGC GAA GTC-3′; H2B-B: 5′-ACG CGT TTA AAC CTT AGC GCT GGT GTA CTT GGT G-3′ and cloned into the C terminal HaloTag Flexi vector pFC14A (Promega Corp.) by digesting the PCR product and the vector with the same enzymes used for the p53 clones.

All the resulting constructs were checked by DNA sequencing.

Cell culture, transfection and fluorescent labeling

Lung carcinoma H1299 cells, which are p53 null, were grown at 37°C and 5% CO_2 in RPMI-1640 medium (Gibco BRL, Gaithersburg, MD, USA) supplemented with 10% fetal bovine serum, 1% glutamine and 0.5% penicillin-streptomycin. Prior to experiments, cells were transferred to LabTek chambers (Thermo-Fisher Scientific, Roechester, NY, USA) in Phenol-red-free complete D-MEM (Invitrogen, Carlsbad, CA, USA) and transiently transfected using Lipofectamine LTX (Invitrogen) according to the manufacturer's instructions. 12 hours after transfection, the cell permeable fluorescent ligand HaloTag-TMR (Promega Corp.) was added to the wells at concentrations of 5 nM for SMT, 50 nM for FCS and 500 nM for FRAP. After an incubation period of 30 min and extensive washing (3 times for 20 min) with Phenol-red-free complete D-MEM (Invitrogen) to remove the unliganded fluorescent molecules, the cells were then mounted on the microscope.

SMT microscopy

The widefield microscope for the collection of the single molecule tracking data was custom-built based on a previously described design (24). Exemplary acquisitions for p53-wt and for the H2B constructs are provided in Supplementary Movie 1 and 2, respectively. The collected movies were analyzed by custom-written Matlab (Mathworks, Natick, MA, USA) routines to identify and track individual molecules. The analysis routines are publicly available at: http://code.google.com/p/single-molecule-tracking. Details of the imaging setup and of the SMT data analysis are provided in the Supplementary Methods and in Supplementary Figures S1 and S2.

Calculation of displacements, MSD, and displacement histogram

The single molecule trajectories were analyzed by measuring the distances jumped, r, at different time-lags ($t = m\Delta t$ with m an integer, and Δt the time between consecutive images). The resultant displacements for different tracks were then used to either calculate an ensemble-averaged mean-squared displacement (MSD) curve (25) or to populate a time-dependent histogram of displacements (26), or in other words the distribution of jumps obtained at different time lags $t = m\Delta t$.

For the histogram of displacements, the size of the bins, Δr, was chosen to be 20 nm, slightly smaller than the accuracy in single-molecule localization, 27 nm (see section 'Results'). We normalized this histogram to the total number of jumps measured at the shortest time-lag, $t_1 = \Delta t$. The normalized histogram, $p(r,t)\Delta r$ which was corrected for photobleaching as described below, represents the probability of observing a displacement between $r - \Delta r/2$ and $r + \Delta r/2$ in a time t.

For p53-wt, the MSD plot was separately calculated for the track segments identifying bound or free molecules. The MSD plot for free p53-wt molecules was fit either with a simple diffusion model, $MSD = 4Dt$, where D represents the diffusion coefficient, or with a hindered (anomalous) diffusion model, $MSD = 4\Gamma t^{\alpha}$, where α is the anomaly parameter and Γ is a proportionality constant (27).

Identification of bound and free molecules using objective thresholds in SMT

To provide a direct estimate for the average residence time of p53 without relying on kinetic modeling, we used H2B data to define an upper threshold for the displacements between two consecutive frames, $r_{\max} = 220$ nm, to identify the molecules that were bound to chromatin. 99% of the H2B displacements were below this threshold.

For each p53 track we identified the jumps satisfying $r < r_{\max}$ and we counted the number of consecutive frames that met this criterion, to obtain the duration t_i of each binding event. We then computed the cumulative histogram $S(t)$, drawn from the occurrences of $t_i > t$. The normalization of $S(t)$ to $S(0) = 1$ yields the probability of having a molecule still bound after a time t, called the survival probability. At short times the survival probability $S(t)$ is contaminated by slowly diffusing free molecules jumping short distances. We therefore analyzed the survival probability only for particles jumping less than $r_{\max}$ for more than a certain number $N_{\min}$ of consecutive frames. We chose a sufficiently large value of $N_{\min}$ such that slowly diffusing free molecules minimally contaminate the selected trajectories, $N_{\min} = 16$ frames (see section 'Results'). We can calculate the probability that a free molecule with diffusion coefficient D_f will be erroneously counted as bound as:

$$P(r_{\max},N_{\min}) = \left(1 - e^{-\frac{r_{\max}^2}{4D_f\Delta t}}\right)^{N_{\min}}$$

For the selected thresholds, $P(r_{\max},N_{\min}) < 0.01$ for $D_f > 0.2\,\mu m^2/s$. To further decrease the contamination from freely diffusing molecules we neglected all the tracks jumping more than the maximum displacement observed for H2B over $N_{\min}$ frames. The resultant survival probability was corrected for photobleaching as described below, sampled logarithmically to avoid overweighting of the counts-poor distribution tail and fitted to an exponential decay to estimate the average residence time of bound p53-wt molecules.

Fitting of SMT displacement histograms with kinetic models for diffusion and binding

We developed kinetic models accounting for diffusion and binding that could be fit to the displacement histograms generated by SMT (Supplementary Note). The models assumed that the chromatin bound state diffused either at an unknown rate or at the rate measured for H2B ($D = 0.0019\,\mu m^2/sec$), and that molecules could exchange between this slowly diffusing state and either one or two freely diffusing states with an unknown diffusion constant(s). The exchange rates between the slowly diffusing state corresponding to bound molecules and the freely diffusing state(s) corresponding to free molecules were given by two additional unknown parameters, the association and dissociation rates of binding. The models were implemented in Matlab (Mathworks, Natick, MA, USA) and fit to the p53 data via non-linear least squares minimization, performed with custom-written routines based on the lsqnonlin function. The models provided estimates of the free diffusion constant(s) and the association and dissociation rates of binding, whose inverse are respectively the average search time for a binding site τ_s and the average residence time on chromatin τ_b. The fraction of bound molecules C_{eq} is then calculated as $C_{eq} = \tau_b/(\tau_b + \tau_s)$. The error bars on the estimated parameters correspond to the 95% confidence intervals. The kinetic models for the SMT displacements histograms were validated by Monte Carlo simulations (see Supplementary Note).

Photobleaching correction for displacement distribution and residence time histograms

Photobleaching of the fluorescently labeled single molecules affects the histogram of displacements $p(r,t)\Delta r$ and the survival probability of bound molecules $S(t)$, in both cases resulting in a decrease of the number of counts over time.

The photobleaching decay can be directly estimated from the single molecule movies, by plotting the number of detected particles (accumulated in the different cells) as a function of time. The decay was fit to a bi-exponential decay:

$$B(t) = f_{b,1}e^{-k_{b,1}t} + (1 - f_{b,1})e^{-k_{b,2}t}$$

to obtain the photobleaching rates $k_{b,1}$ and $k_{b,2}$ together with the corresponding fractions $f_{b,1}$ and $1 - f_{b,1}$. The distribution of displacement and the survival probability were then normalized for photobleaching by dividing

$p(r,t)\Delta r$ and $S(t)$ by $B(t)$. To test the validity of the photobleaching correction we collected SMT data at two different photobleaching rates. The photobleaching rate was tuned by varying the time between exposures (when the laser is not delivered to the sample), resulting in frame rates of 25 Hz to 10 Hz. After photobleaching correction $S(t)$ was found to be independent of the acquisition rate (Supplementary Figure S3b), resulting in very similar estimates for the p53-wt residence time, thus validating our photobleaching correction. Similarly, the estimated binding parameters from the photobleaching-corrected histograms of displacements for p53-wt did not depend on the acquisition (and photobleaching) rate (Supplementary Table S1).

FRAP and FCS

FRAP and FCS were performed as described in (6) and (28), respectively. See Supplementary Methods for details.

RESULTS

Different analyses of FRAP, FCS and SMT data generate widely discrepant estimates for p53 binding in live cells

To establish a benchmark for live-cell binding we have applied FRAP, FCS and SMT to the same transcription factor p53 (Figure 1a) analyzed in the same p53-null human cell line (H1299) in the absence of DNA damage. We transfected H1299 cells with p53 fused to a HaloTag receptor (29). The fused receptor is comparable in size to GFP but binds to a fluorescent tetramethyl-rhodamine (TMR) ligand that is membrane permeable. This has several advantages for the comparative analysis performed here. The same transfected protein concentration can be used for FRAP, FCS and SMT, but optimal levels of fluorescence for each technique (high for FRAP, medium for FCS and low for SMT) can be achieved by simply altering the concentration of the TMR ligand. The chosen ligand concentrations resulted in different fractions of labeled p53 molecules, namely ~80% for FRAP, ~25% for FCS and ~5% for SMT (Supplementary Results). Furthermore, we found that TMR was at least 15 times more photostable than GFP (Supplementary Figure S1c). This has significant advantages for performing SMT where bleaching of the genetically encoded fluorescent proteins like GFP is a serious limitation to obtaining tracks of sufficient length for quantitative analysis (30).

Using the Halo-tag fusion of p53 we collected live-cell binding data for FRAP, FCS and SMT. To analyze these data, we applied three widely used kinetic models for FRAP and FCS and three different criteria for selecting thresholds to identify bound molecules in SMT. We obtained p53 residence time estimates that ranged from 0.02 to 6 s and bound fraction estimates that ranged from 20 to 100% (Figure 1b–d). This divergent range of estimates recapitulates the widely discrepant predictions that have been obtained for an assortment of proteins using these different live-cell binding procedures.

SMT estimates of p53 binding can be reconciled by objective selection of bound molecules

To reconcile the different predictions from the analyses of FRAP, FCS and SMT data, we began with SMT since it is the most direct measurement, and developed two independent procedures to estimate residence times and bound fractions by SMT.

First, we re-examined previous thresholding approaches in SMT (10,23) which have been used to identify bound molecules based on the minimum number of timepoints N_{min} for which a molecule remains within a maximal displacement r_{max}. Studies of chromatin binding by SMT have chosen r_{max} based on the presumption that bound molecules were immobile. To test this, we performed SMT on histone H2B which is known to be tightly bound to chromatin (31) and measured a maximal displacement of $r_{max} = 220$ nm (Figure 2a). This displacement is much larger than our precision limit of localization in SMT, 27 nm, as determined by the MSD plot in fixed cells (Figure 2c), and instead is consistent with the fact that chromatin diffuses slowly (32). Thus we used this empirically determined value of r_{max} from H2B to set the maximum displacement for declaring a p53 trajectory segment as bound.

To determine a value for N_{min}, the minimum number of time points for a bound trajectory in SMT, we set $r_{max} = 220$ nm for the p53 SMT data and then varied N_{min} (Figure 2b). The estimated residence time for p53 plateaued at $N_{min} = 16$ time-points, which presumably reflects a sufficiently large enough value of N_{min}, such that slowly diffusing free molecules no longer contaminate the selected trajectories. We selected this value of N_{min} as the minimum number of time points for declaring a p53 trajectory segment as bound and using these thresholds we estimated that 19% of the p53 molecules are bound at any time with an average chromatin residence time of 1.7 s (Table 1).

As a self-consistency check of these empirically determined objective thresholds ($r_{max} = 220$ nm and $N_{min} = 16$ time-points), we performed an analysis of the MSD of the putatively bound p53 molecules compared with all H2B molecules. These two MSD plots overlapped at long times (>0.2 s), but the MSD plot for p53 was higher than that for H2B at shorter times (Figure 2c). This indicates that the chromatin bound by p53 diffuses somewhat faster than the more generic chromatin bound by H2B. Such a difference could arise for a variety of reasons, e.g. p53-bound chromatin may contain less nucleosomes and so diffuse faster than generic chromatin (33). Regardless of its cause, this difference indicates that the objective thresholds that we should use to define p53-bound molecules should be somewhat different than the objective thresholds that we determined empirically from H2B bound chromatin. To evaluate the potential impact of this on our p53 binding estimates, we varied the values of the objective thresholds (r_{max} and N_{min}) applied to our p53 SMT data. We found that there was less than a 30% difference in the p53 binding estimates, as long as N_{min} and r_{max} were chosen large enough to exclude contamination from free molecules (Supplementary Figure S3a).

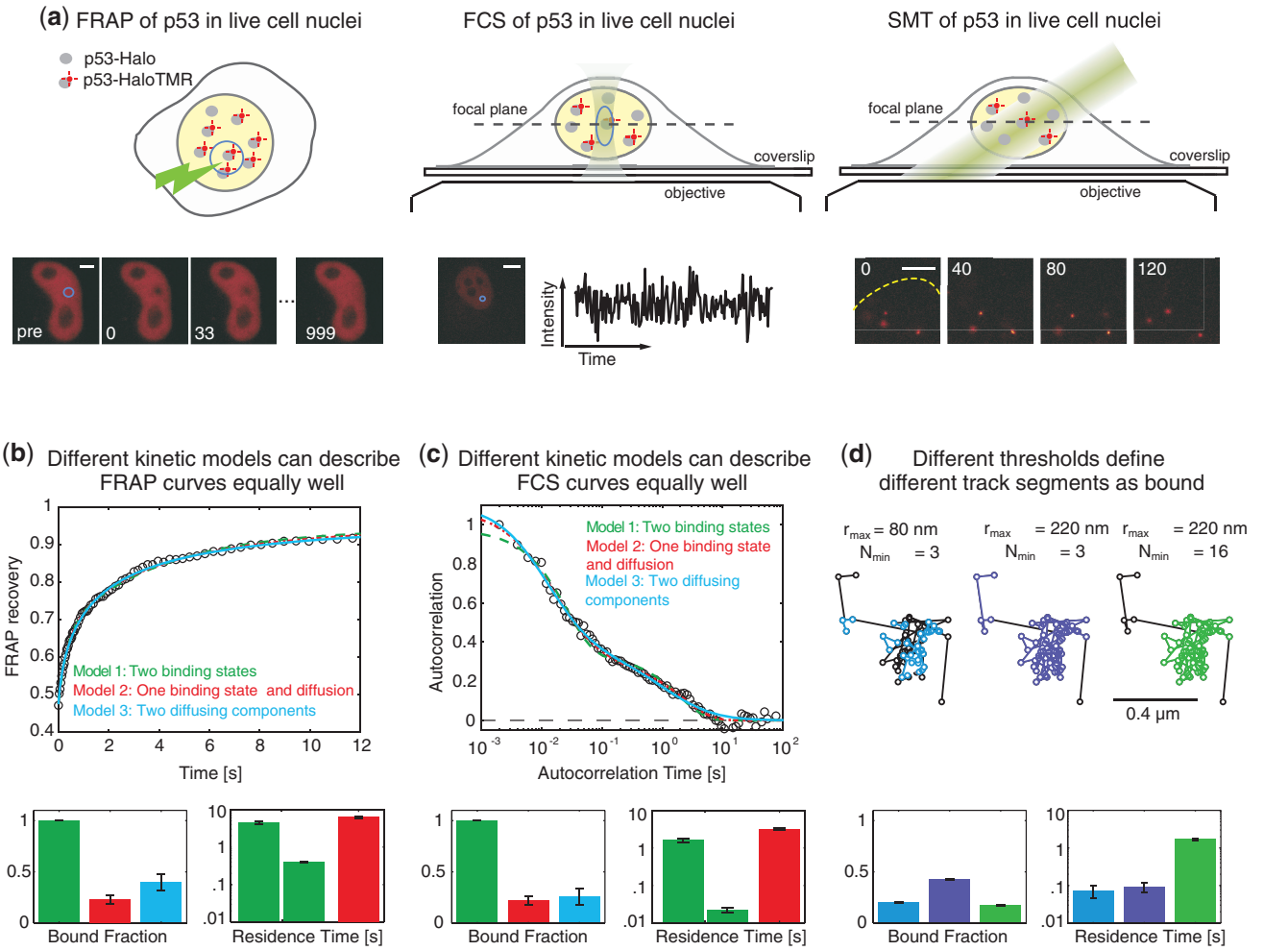

Figure 1. Differences in FRAP, FCS and SMT analysis result in discrepant binding estimates. (**a**) FRAP, FCS and SMT were performed on a p53 construct fused with a Halotag receptor transiently transfected in the human H1299 p53-null cell line. The tetramethylrhodamine (TMR) ligand (red cross) is membrane permeable and binds covalently to the HaloTag fusion protein (grey circle). The ligand concentration can be adjusted depending on the technique. FRAP and FCS were performed on a commercially available confocal microscope, while SMT was performed on a custom-built widefield microscope using an inclined illumination scheme (See also Supplementary Figure S2). The numbers in the image sequences represent the acquisition time in ms. The scale bar corresponds to 5 µm. The blue circle in the first image of the FRAP sequence (left) represent the bleached area. The blue square in the FCS image (center) represents the location of the FCS observation volume. (**b**) The FRAP data could be fit equally well by three different models: (1) a model accounting for two binding states and no diffusion (green line); (2) a model accounting for one binding state and one diffusion state (red line); (3) a model accounting for two diffusion states (blue line). The different models resulted in discrepant estimates of residence times, ranging from 0.4 to 6.3 s and bound fractions, ranging from 23 to 100% (error bar SEM $n = 27$). (**c**) FCS data obtained on p53-wt-HaloTag are also well fit by any of the three models in (b), resulting in residence times ranging from 0.02 to 3.2 s and bound fractions ranging from 22 to 100% (error bars SEM $n = 15$). Note that only model (2) provides reasonably self-consistent estimates by FRAP and FCS. (**d**) Binding parameters are isolated from the single molecule tracks by defining the bound molecules as those tracked for at least N_{min} consecutive frames yielding frame-to-frame displacements less than r_{max}. The same track (black) is shown in each case, but the segment(s) of the track identified as bound (blue purple, green) depends on the threshold used. Applying these same thresholds to all of the p53 tracks results in residence times ranging from 0.05 to 2 s and bound fractions ranging from 10 to 40% (error bars are 95% confidence intervals).

Thus, this suggests that only relatively small errors will be introduced by assuming that p53-bound chromatin behaves identically to H2B-bound chromatin.

Kinetic modeling of SMT yields independent estimates of p53 binding consistent with objective thresholding

To increase our confidence in the binding parameters estimated by objective thresholding, we developed a kinetic modeling procedure as a second, independent approach to estimate residence times and bound fractions from the p53 SMT data. Our kinetic model incorporated both diffusion and binding (See Supplementary Note), and so provided a description of all p53 trajectories. Importantly, the model did not require threshold selection to distinguish bound from free molecules, but rather included the diffusion of the p53-bound molecules D_b which was either fixed to the value obtained for H2B or

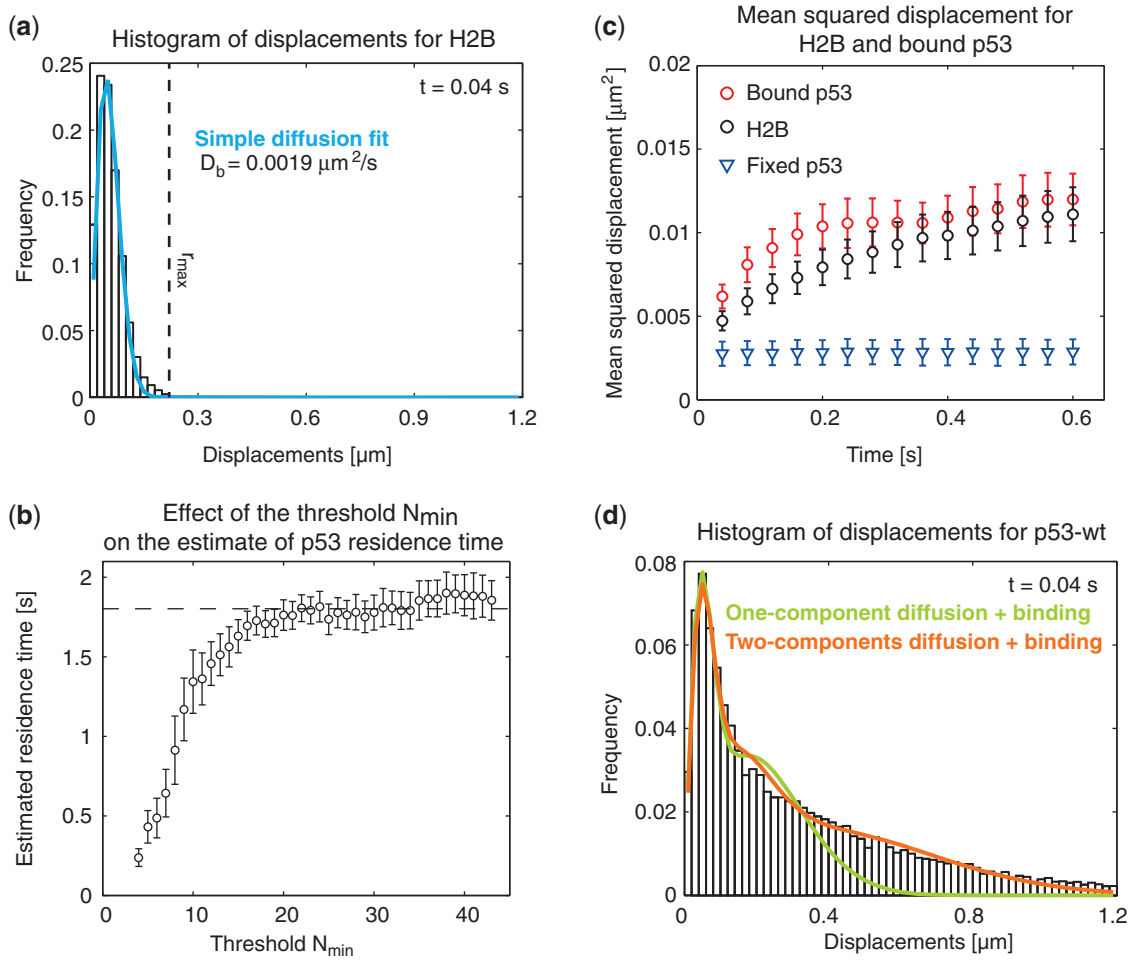

Figure 2. Analysis of the SMT data for H2B and p53. (**a**) We performed SMT on histone H2B, which is tightly bound to chromatin. The histogram of displacements was calculated at all possible time lags between frames of the single molecule movie, but for clarity only one time lag of the full 2D histogram is shown, $t = 0.04$ s. (Histograms at different time lags are shown in Supplementary Figure S4). The histogram at $t = 0.04$ s shows a peak at a displacement of ~50 nm, with 99% of the displacements shorter than 220 nm. The histogram was well described by a diffusion model, resulting in an estimate for the diffusion of the chromatin-bound H2B molecules equal to 0.0019 $\mu m^2/s$. (**b**) We chose the maximum H2B displacement observed between consecutive frames r_{max} as a threshold to define chromatin bound molecules. However, as some free p53 molecules can diffuse slowly enough to mimic binding, we discarded p53 track segments with displacements less than r_{max} for shorter than a minimum number of frames N_{min}. The estimated p53 residence time increases for higher values of N_{min}, until a plateau is reached at N_{min}~16 frames, corresponding to a situation where the probability for a free molecule (with a diffusion coefficient $D > 0.2\ \mu m^2/s$) to be counted as bound is less than 1%. (**c**) We therefore used $N_{min} = 16$ frames and $r_{max} = 220$ nm to select bound p53 molecules. We compared the MSD plot for the putative bound p53 molecules (red circles) and to the MSD plot obtained for all the histone H2B molecules (black circles). Although the plots show considerable overlap, at early times the bound p53 molecules diffuse faster, suggesting that there are some differences between chromatin bound by p53 versus H2B. Control experiments on fixed samples (blue triangles) yielded a flat MSD curve, which we used to estimate the localization accuracy of the system σ as (51): $MSD = 4\sigma^2$, resulting in $\sigma = 27$ nm. (**d**) Like H2B, the time-dependent histogram of displacements for p53 also shows a peak at ~50 nm, which likely reflects chromatin-bound molecules. However, the p53 histogram exhibits a much longer tail than the H2B histogram. The full 2D histogram for p53 was fit with two different kinetic models, but for clarity the fit at only one time lag of the full 2D histogram is shown, $t = 0.04$ s (16 221 jumps). (Fitting results at other time lags are shown in Supplementary Figure S5). The estimated binding parameters from the fits are provided in Table 1.

kept as a free parameter to be determined from the data. A second free parameter in the model was the diffusion rate of free p53 molecules. Finally, the model also contained two other free parameters, the association and dissociation rates of binding that specified the exchange between the bound and free states.

This kinetic model was applied to fit the complete set of p53 displacements obtained from all trajectories (Figure 2d) and this yielded an estimated bound fraction and residence time that were similar to those estimated using the thresholding procedure (Table 1) both when D_b was fixed to the value obtained from the H2B data or when D_b was kept as a free parameter. In the latter case, the estimated diffusion constant for bound p53 molecules was faster than that measured for H2B (0.0027 $\mu m^2/s$ versus 0.0019 $\mu m^2/s$), consistent with our comparison of the MSD plots for bound p53 versus H2B molecules (Figure 2c). Thus, the kinetic model and the objective thresholding procedure yield very similar conclusions.

While the preceding kinetic model yielded a good fit to the smaller p53 displacements (which reflect bound molecules), the fit was poor for the larger displacements

Table 1. Estimated p53-wt diffusion and binding parameters from the analysis of the SMT data by objective thresholding and kinetic modeling

	τ_b [s]	C_{eq} [%]
Objective thresholding	1.7 ± 0.2	19 ± 2
Kinetic modeling—One component diffusion and binding (Fixed D_b)	1.34 ± 0.16	28 ± 8
Kinetic modeling—One component diffusion and binding (Variable D_b)	1.49 ± 0.15	28 ± 7
Kinetic modeling—Two component diffusion and binding (Fixed D_b)	2.2 ± 0.3	17 ± 5
Kinetic modeling—Two component diffusion and binding (Variable D_b)	2.3 ± 0.3	19 ± 5

We quantified the binding behavior of p53-wt by analyzing SMT data obtained at a frame rate of 25 Hz with two different methods: objective thresholding to select the bound molecules and kinetic modeling of the histogram of displacements. Independently of the model chosen to describe the behavior of the free population (one or two components) and of the choice of fixing the diffusion coefficient of the bound population, the estimated residence time and bound fractions are compatible with the results obtained by objective thresholding. τ_b is the estimated residence time. C_{eq} is the estimated bound fraction (errors: 95% confidence intervals).

(which reflect free molecules). To investigate whether improving this fit to the larger displacements would influence the binding estimates, we added a second freely diffusing state to the kinetic model. This added two more free parameters to the model, namely the diffusion constant of this second freely diffusing state and the fraction of molecules in this state. As expected with the addition of more free parameters, the new kinetic model yielded a better fit to the p53 displacement histogram. However, the estimates for the p53 bound fractions and residence times were not significantly changed. This provides further confidence that our binding estimates from SMT are reasonably accurate.

It is important to point out that the good fit of the SMT data obtained by presuming two freely diffusing components does not prove that two such states actually exist. Instead, it is likely that these two states provide a simple way to fit the more complex anomalous diffusive processes that are known to occur within nuclei (32). Consistent with this possibility, we found that the MSD plot for the unbound p53 could be fit with an anomaly exponent $\alpha = 0.82$ (Figure 3b) that matched the anomalous diffusion found for inert tracers, such as quantum dots, inside the nucleus (27). One simple explanation for this anomalous diffusion in the nucleus is that it arises from hindered diffusion due to chromatin obstacles (27,34).

Although much more analysis will be necessary to determine if chromatin obstacles can adequately explain the complex diffusion of p53, our data suggest that the details of this diffusion are not important for estimating the binding properties of p53. This is because we obtained very similar binding estimates regardless of whether we treated p53 diffusion by objective thresholding, a one-component diffusion model or a two-component diffusion model. This robustness of SMT to the diffusion model presumably reflects the fact that the displacements of bound molecules in SMT are in general well separated from those of free molecules, and consequently the estimates of binding parameters are not overly sensitive to the details of the procedure used to characterize diffusion of the free molecules.

As a final validation of our method, we showed that the estimated residence times and bound fractions were not dependent on either the data acquisition rate, which was varied from 10 to 50 Hz (Supplementary Table S1) or on the photobleaching rate (Supplementary Figure S3b). In sum, using both kinetic modeling and objective thresholding, we have obtained independent, but consistent estimates of bound fractions and residence times by SMT.

SMT data can be used to identify the correct kinetic model for FRAP and FCS

We then asked how these consensus SMT estimates compared to the FRAP and FCS estimates. These varied widely depending on the kinetic model applied (Figure 1b–d), so we used the SMT data to help select the most appropriate kinetic model for p53. For binding, the FRAP and FCS kinetic models assumed either zero, one or two binding states. However, we found that the distribution of p53 residence times obtained by thresholding the SMT data to select bound molecules was well fit by a single exponential (Figure 3a). This suggests that a single-binding state should be sufficient for the FRAP and FCS kinetic models, a result consistent with our observation that a single-binding state kinetic model was sufficient to explain the small displacements in the p53 displacement histogram obtained by SMT. Thus the SMT data, whether analyzed by objective thresholding or by kinetic modeling, point to a one-binding-state model for p53 as the appropriate one for FRAP or FCS analysis.

To investigate the role of diffusion in the p53 kinetic models, we examined all of the p53 molecules analyzed by SMT that did not satisfy the thresholds for bound molecules, and so by definition were free. Using these data, we generated an MSD plot for free p53 molecules, and used it to calculate how long a typical free p53 molecule would take to diffuse across our FRAP or FCS measurement spots (Figure 3b and Supplementary Methods).

For our FRAP spot size (2 μm in diameter) the time required for a free molecule to equilibrate was $\tau_{D,FRAP} = 0.28$ s. This time to diffuse across the FRAP bleach spot is only 20x faster than the time to bind a site, which can be calculated (see Supplementary Methods) from the residence times and bound fractions obtained by the SMT analysis. A 20x difference is not fast enough to ignore diffusion in the kinetic model (as incorrectly assumed by the two-binding state model of Figure 1b), since theory indicates (35) that the difference

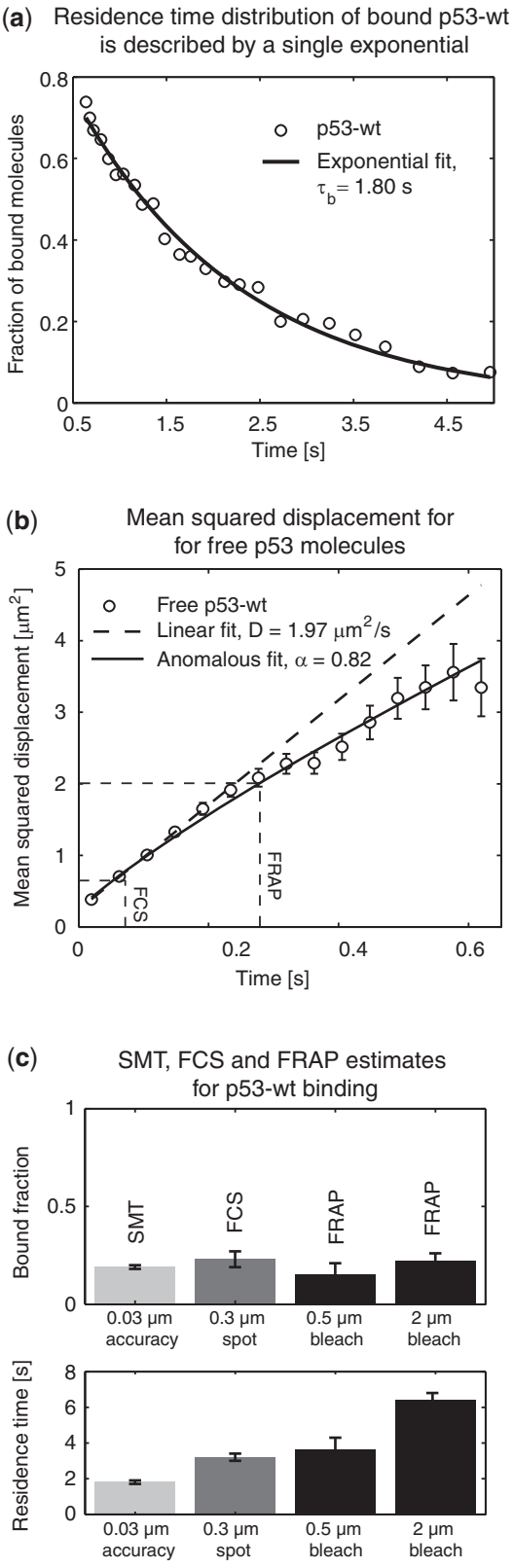

Figure 3. Identification of the proper kinetic model for p53. (**a**) The durations of p53-wt binding events as measured by our objective thresholding of the SMT data were plotted as a cumulative histogram (circles). This was well fit by a single exponential (solid black line), Indicating that a kinetic model for p53 should account for a single binding state. Larger displacements of p53-wt that the objective threshold procedure identified as free yielded an MSD plot (errors SEM, $n > 200$) that was not described by simple diffusion (dashed line), but rather by hindered diffusion (solid line). (**b**) The MSD plot was used to quantify the time p53-wt takes to diffuse through the FRAP spot, 0.28 s and through the FCS volume, 0.07 s. These times indicate that diffusion should be included in the FRAP and FCS kinetic models (see section 'Results'). (**c**) The FRAP and FCS predictions using a kinetic model with one bound state and one diffusing state match the SMT estimates for bound fractions and differ by a factor of four and two, respectively from the SMT estimates for residence times. The differences in residence-time estimates correlate with the spatial resolution of the technique, as confirmed by performing FRAP with a smaller bleach-spot size (error bars: 95% confidence intervals for SMT, SEM., $n = 27$ for FRAP with 2 μm bleach spot, SEM., $n = 24$ for FRAP with 0.5 μm bleach spot, SEM., $n = 15$ for FCS).

should be at least 100x. We conclude that the FRAP kinetic model should incorporate diffusion.

For our FCS spot size (0.3 μm), the time required for a free molecule to equilibrate was $\tau_{D,FCS} = 0.07$ s, which is 100 x faster than the time to bind a site. This indicates that free molecules equilibrate significantly faster than bound molecules in FCS due to the much smaller spot size compared to FRAP. However, in our FCS experiments, the time interval between measurements is 0.002 s, which is sufficiently fast to detect the rapid equilibration of the free molecules. We conclude that the FCS kinetic model should also incorporate diffusion.

The selected kinetic model for FRAP and FCS provides consistent estimates for the three different techniques, with minor differences in the estimated residence time, probably due to hindered diffusion

As described above, the SMT data suggest that the kinetic model for both FRAP and FCS should incorporate diffusion and one binding state. This corresponds to kinetic model 2 in Figure 1b and c. This model yielded FRAP and FCS estimates for the p53 bound fraction that were within error of our consensus SMT estimates, and residence times that were a factor of two larger for FCS and a factor of four larger for FRAP (Figure 3c).

The discrepancy in residence time estimates was correlated with the precision limit of the techniques, with the smallest estimate (1.8 s) obtained by SMT which has a spatial precision of 27 nm, the intermediate estimate (3.2 s) obtained by FCS which has a spatial precision of 300 nm, and the largest estimate (6.3 s) obtained by FRAP which has a spatial precision of 2000 nm. To test this correlation further, we performed FRAP with different bleach spot sizes (Supplementary Figure S6a) and found that the residence time progressively decreased down to 3.4 s at the smallest bleach spot size of 0.5 μm (Figure 3c).

These changes in the FRAP estimate with progressively smaller bleach spots could reflect the fact that the FRAP model presumes that free p53 molecules undergo simple diffusion with a single diffusing state, whereas our analysis by SMT suggests that p53 diffusion may instead be anomalous with an MSD plot consistent with hindered diffusion caused by chromatin obstacles. Similar changes in FRAP estimates with different bleach spot sizes have been used to argue for the existence of microdomains

that produce hindered diffusion in plasma membranes (36). To test if hindered diffusion could influence our binding estimates we performed Monte Carlo simulations and found that FRAP models that ignore hindered diffusion introduce artifactual bound states for large but not small bleach spots (see Supplementary Methods and Supplementary Figure S6b–d). Thus these data together suggest that by ignoring hindered diffusion FRAP models may compensate for this error by increasing the estimated residence times.

In sum, we used direct analysis of single molecule trajectories to infer that kinetic models for FRAP and FCS should include one binding state and diffusion. This yielded bound fractions of ~20% for FRAP, FCS and SMT, and residence time estimates that differed by at most a factor of two when using a small bleach spot size in FRAP. Monte Carlo simulations suggested that the remaining difference in residence time estimates may be due to ignoring hindered diffusion in the FRAP and FCS kinetic models.

The measured p53 bound fraction includes contributions from sequence-specific and sequence-independent binding

Different live-cell binding studies have interpreted the bound fraction of transcription factors as reflecting either sequence-specific binding, sequence-independent binding or some combination of the two. To investigate this question for p53, we performed single molecule tracking of p53 mutants which are thought to affect either specific or sequence-independent binding via the p53 core domain or C-terminal domain respectively, and compared them to wild-type p53 (Figure 4a). We first analyzed the effect of a point mutation (p53-R273H) in the DNA binding core domain of p53 that strongly suppresses DNA binding to specific-site sequences, as indicated by chromatin immunoprecipitation (37). From the analysis of the single-molecule histogram of displacements (Figure 4b) for this specific-site-binding mutant we estimated a bound fraction of 11% (Table 2), corresponding to a loss of about 40% of the bound fraction measured (18%) for the wild-type p53 at the same frame rate (50 Hz). Further, the R273H mutant displayed a 2-fold reduction in the residence time (Table 2), suggesting that the longer residence times measured may correspond to sequence-specific binding interactions with DNA.

We then analyzed the behavior of a p53 mutant (p53-d30) lacking the last 30 amino-acids of the p53 C-terminal domain (Figure 4c). This mutant has been shown *in vitro* to strongly compromise the sequence-independent interactions of p53 and its sliding on DNA (38). This sequence-independent binding mutant showed an even larger drop of the p53 bound fraction to 6% (Table 2), corresponding to a loss of about 65% of the total bound fraction. Thus the reductions in the bound fractions for the sequence-independent mutant (65%) and the site-specific mutant (40%) total ~100%, raising the possibility that these two domains of p53 are responsible for most of its DNA binding. This hypothesis however was not confirmed by single molecule tracking of a double mutant p53-R273H/d30, which showed a residual bound fraction of 6% (Table 2), identical to what we measured for the C-terminal domain mutant p53-d30. Similarly, the distribution of displacements observed for p53-d30 alone and the p53-d30/R273H (Figure 4c and d, respectively) were nearly identical. Therefore, the double mutant retains some ability to transiently interact with DNA, probably through other p53 domains. Further, our data show that the DNA binding mediated by the site-specific and sequence-independent domains is not independent, as the p53-d30 mutation by itself was capable of disrupting the same amount of binding as when the combination p53-R273H/d30 was used. Together these data suggest a binding pathway, with p53 sequence-independent binding required for p53 site-specific binding.

DISCUSSION

Cross validation of live-cell binding measurements

We have demonstrated how to achieve consensus among three different approaches to measure live cell binding of p53 to chromatin. This provides confidence that our current estimates are reasonably accurate, and it also provides guidance for the future on how to make these measurements accurately for other molecules bound to either chromatin or other cellular scaffolds such as the cytoskeleton and cellular membranes (4,39). Specifically, we found excellent agreement among SMT, FRAP and FCS estimates for bound fractions which were within error, and very good agreement for residence time estimates which differed by a factor of two when small spot sizes were used in FRAP (Figure 3c). We also showed that the small error in residence time estimates is likely due to ignoring hindered p53 diffusion in the FRAP and FCS kinetic models.

We believe that of the three estimates, the SMT estimate is the most reliable since it is both direct and robust to the methods used to analyze the SMT data (Table 1). Further, by SMT we were able to quantify behaviors that were not directly visible by ensemble average techniques like FRAP and FCS. For example, by SMT we found that chromatin-bound p53 exhibited slow diffusion and that free p53 exhibited hindered diffusion, probably due to chromatin obstructions.

We used the SMT data to deduce that a minimal FRAP or FCS kinetic model should include one binding state and diffusion. Previous FRAP studies of p53 had used several less direct tests to infer that diffusion should be incorporated into the kinetic model (6,12). Our analysis now indicates that these tests for diffusion are accurate and valuable for determining its role in a kinetic model. Thus our current analysis by FRAP, and these two previous FRAP analyses, have all applied the same reasonably accurate kinetic model yielding similar estimates for p53 residence times and bound fractions (6,12).

Despite the achieved consensus, the SMT data showed that a model with one binding state and diffusion is flawed for the case of p53 since it does not account for either the hindered diffusion of unbound molecules or the slow diffusion of bound molecules. Nevertheless, we found that if

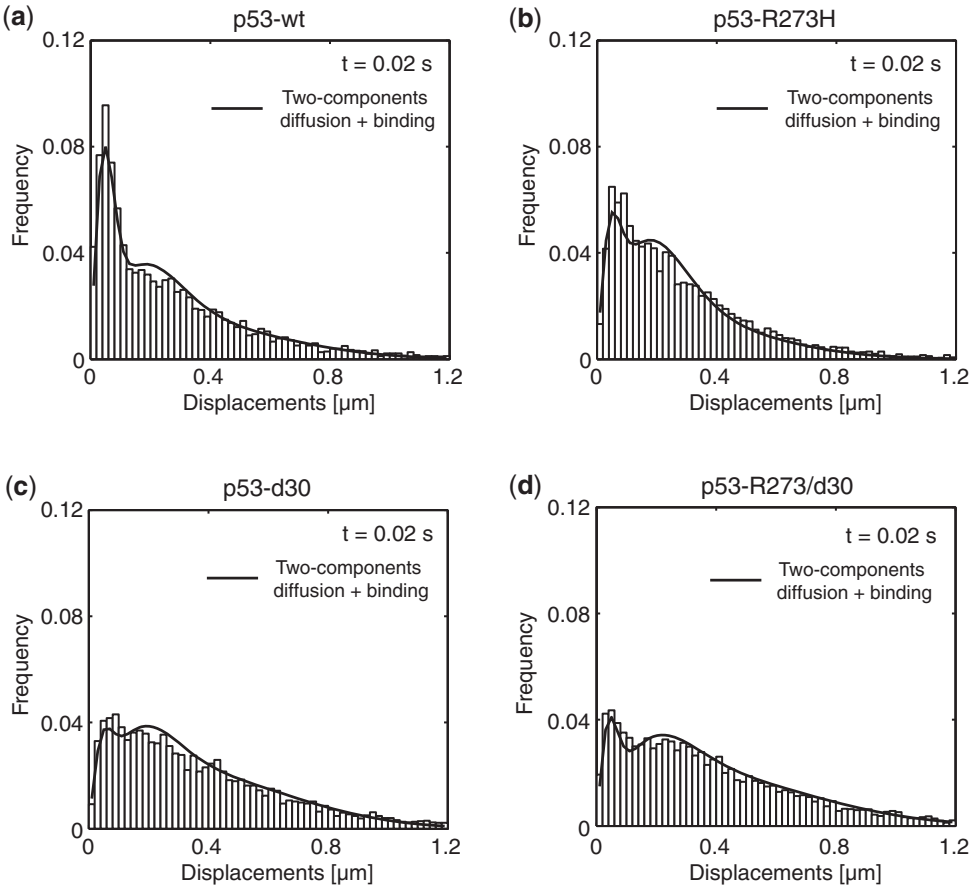

Figure 4. Comparison of wild-type and mutant p53 displacement histograms. The histogram of displacements for p53-wt obtained at a frame rate of 50 Hz (**a**) was compared to the one obtained for a mutant (p53-R273H) known to suppress binding to specific sites (**b**), a mutant (p53-d30) known to suppress binding to non-specific DNA sequences (**c**) and a double mutant p53-R273H/d30 (**d**). All mutants resulted in a drop of the peak at short displacements corresponding to bound molecules. Interestingly, the histograms for the p53 double mutant and p53-d30 were very similar, indicating that p53-d30 not only affected the sequence-independent interactions but also suppressed binding to specific sites. Fitting of the histograms with a model accounting for two free populations exchanging with one bound population resulted in the estimates of the bound fractions and residence times reported in Table 2.

Table 2. Comparison of the diffusion and binding estimates for p53-wt and mutants obtained by kinetic modeling of the SMT histogram of displacements

	D_1[μm^2/s]	D_2[μm^2/s]	f_1	τ_b [s]	C_{eq} [%]
P53-wt	3.4 ± 0.8	0.66 ± 0.14	0.48 ± 0.02	1.72 ± 0.11	17.6 ± 2.6
p53-R273H	2.7 ± 1.5	0.61 ± 0.41	0.41 ± 0.03	0.90 ± 0.08	10.5 ± 2.1
p53-d30	3.8 ± 0.5	0.63 ± 0.13	0.66 ± 0.01	0.20 ± 0.02	5.5 ± 1.2
p53-R273/d30	4.4 ± 0.6	0.81 ± 0.12	0.67 ± 0.02	0.48 ± 0.04	6.5 ± 0.8

We compared the histograms of displacements obtained at a frame rate of 50 Hz for p53-wt, for a mutated form of p53 unable to bind to specific sequences (p53-R273H), for a truncated form of p53 mutant with impaired sequence-independent interactions with DNA (p53-d30) and for a construct with both mutations (p53-R273H/d30). The histograms of displacements were fit with a model accounting for two free diffusing components exchanging with a chromatin bound component. D_1 and D_2 are the estimated diffusion coefficients associated to the two free components. f_1 is the fraction of molecules diffusing with the first diffusion coefficient. τ_b is the estimated residence time. C_{eq} is the estimated bound fraction (errors: 95% confidence intervals). Note that the diffusion coefficients obtained for all the mutants are smaller than what expected from the size of a Halo-p53 tetramer, 7–10 μm^2/s, as calculated as described in (8), using a diffusion coefficient for nucler GFP equal to 15 to 20 μm^2/s.

the basic framework of the kinetic model was accurate (one binding state and diffusion for p53), then these other errors in the kinetic model led to relatively small errors in the estimates of p53 residence times by FRAP and FCS.

We also found that with a reasonably accurate kinetic model, the FRAP and FCS estimates by themselves showed reasonable agreement, whereas with incorrect kinetic models the FRAP and FCS estimates were radically different. This might suggest that direct comparison of FRAP and FCS without performing SMT might be sufficient to obtain reliable estimates, however we think this is risky for several reasons. First it is possible that the wrong

kinetic model could by chance yield consistent results for both and FRAP and FCS, and second errors in FRAP or FCS estimates could be larger for other molecules or other cell types, if these exhibit even more hindered diffusion than p53. Thus we recommend using SMT to obtain direct estimates, and also using it to validate the model used in FRAP or FCS. The risk of using an invalid kinetic model to fit FRAP or FCS data is illustrated by the very significant errors in binding estimates that we found if the number of bound states and diffusing states in the kinetic model was incorrect (Figure 1).

The roles of site-specific and sequence-independent binding in p53–DNA interactions

There has been considerable interest in obtaining live-cell binding estimates as these provide insights into the molecular mechanisms of the molecule under study. Here we measured bound fractions and residence times for both wild-type and DNA binding mutants of p53. Below we discuss the implications of each of these measurements for how p53 interacts with chromatin in live cells.

We compared bound fractions of wild-type p53 to three different mutants: p53-R273H which is thought to affect specific-site binding, p53-d30, which is thought to affect sequence-independent binding, and a double mutant p53-R273H/d30, which should affect both. We found that all three mutants reduced the bound fractions relative to wild-type, but the double mutant exhibited the same bound fraction as the single mutant p53-d30. Furthermore, the complete histogram of displacements for the double mutant was also very similar to the single mutant p53-d30. These results argue (by analogy with classic epistasis analysis) that p53-R273H and p53-d30 are involved in the same pathway and that the function of p53-R273H is downstream of p53-d30, since there is no further deterioration in binding when the p53-R273H mutation is coupled with p53-d30. Recently, chromatin immunoprecipitation experiments probing several p53 target sites have also suggested that sequence-independent binding is required as a precursor to p53 sequence-specific binding (40,41). Our results extend these observations and suggest that a pathway from sequence-independent to sequence-specific binding is a general 'genome-wide' mechanism used by p53 to find its targets. More concretely, our data are consistent with the proposal that the C terminal tail (the region deleted in p53-d30) mediates DNA sliding to locate specific binding sites (38).

It is important to point out that the double mutant retains ~5% bound fraction, suggesting that p53-R273H/d30 is still weakly bound to chromatin. This could arise for example if the R273H mutation does not completely eliminate all specific or sequence-independent binding, a distinct possibility given that there are at least seven other residues in the core domain which make DNA contacts. It is also possible that p53 is bound indirectly to chromatin via interactions with co-activator molecules. Further mutagenesis of p53 will be required to determine which domains are responsible for the residual binding still present in the double mutant.

With the current mutant data we can nevertheless make some first estimates of the fractions of p53 molecules bound at specific sites. We found that 18% of p53-wt molecules were bound and that this was reduced by ~7% in the specific-site mutant, implying that ~7% of p53 molecules are bound at specific sites. Therefore our current analysis suggests that some of the binding that we measure by SMT is at specific sites, and that this binding is transient. This is consistent with several FRAP studies of transcription factor binding at artificial and natural tandem gene arrays (42–44), and with the conclusions of a recent SMT study on the activated form of the mammalian transcription factor STAT1 (11).

We estimated that the transiently transfected H1299 cells used for our SMT analysis contained 600–4000 p53 molecules (see Supplementary Results). This range is similar to endogenous p53 levels in unstressed cells (45), suggesting that our measurements were made close to physiological p53 levels. Thus our estimate that 7% of p53 molecules are at specific sites would suggest that prior to stress only ~7% × (600–4000) or ~40–300 specific p53 targets would be occupied in any one H1299 cell. Note however that in normal cells that express p53 these numbers could change radically upon stress. Published estimates suggest that after stress there could be ~80 000 p53 molecules / cell and up to 3000 p53 binding sites genome wide (45–47). If only 7% of these 80 000 molecules were at sequence-specific sites, then 5600 sites could still be occupied which would easily saturate the ~3000 p53 targets. This rough calculation also suggests how the large changes in p53 levels measured before and after stress (up to 20-fold) (46) could provide a simple way to switch p53 target-site occupancy within individual cells from sparse to saturated.

Our analysis of residence times in p53-wt and the different mutants showed that each mutant reduced the average residence time relative to wild-type, but the residence times for the mutants in specific-site versus sequence-independent binding were not radically different. It should be noted that the short residence times for the mutants may be subject to some error, since the estimated residence times are close to our data acquisition rate. Regardless of the precise values for these residence times, our data suggest that the range of residence times we measured for p53 wt (Figure 3a) reflect a continuum of affinities that includes both sequence-specific and sequence-independent binding, but for the mathematical purposes of a kinetic model can be described reasonably well by a 'single binding state' from which we can obtain an average residence time of about 2s for p53 molecules bound to chromatin.

In principle, it is possible that there is a much more transient form of DNA binding presently hidden in what we measure as p53 diffusion. This combination of fast binding and diffusion is known as effective diffusion (35), and it produces a slower diffusion constant than expected from the molecule's size. Indeed, our SMT estimates of the p53 diffusion constant were somewhat slower than expected based on p53's molecular weight (Table 2), but it does not appear that this slowdown is due to very transient DNA binding interactions. If it were, then our

estimate of *D* should have changed in either the specific or sequence-independent mutant. Instead we found similar estimates for *D* for the two mutants and wild-type, suggesting that the somewhat slower value of *D* for p53 probably reflects the formation of either a molecular complex or hindered diffusion rather than binding to chromatin. Thus, in contrast to what has been found for the lac repressor in *Escherichia coli* (2), our current data for p53 suggest a continuum of chromatin residence times, rather than two distinct populations of residence times corresponding to sequence-specific and sequence-independent binding.

We conclude that SMT with HaloTag fusion proteins provides a relatively straightforward and reliable procedure to measure bound fractions and residence times at cellular scaffolds within live cells. We recommend its application in combination with either FRAP or FCS, which should be applied as a cross validation to ensure accurate estimates of binding with the SMT data used to guide selection of a FRAP or FCS kinetic model. The methods we describe here can now be used to estimate binding residence times for either new investigations of live cell binding or re-investigation of previous analyses.

SUPPLEMENTARY DATA

Supplementary Data are available at NAR Online: Supplementary Table 1, Supplementary Figures 1–7, Supplementary Methods, Supplementary Results, Supplementary Note, Supplementary Movies 1–2 and Supplementary References [6,8,24,28,48–54].

ACKNOWLEDGEMENTS

We are grateful to Dr. E.A. Fortunato for providing the p53-GFP plasmids, to Dr. U. Kubitscheck, Dr. T. Meckel and W.G. Mueller for preliminary SMT experiments, to Dr. A. Berezhkovskii, Dr. L. Dagdug, Dr. S. Pajevic and Dr. G. Weiss for discussion of the SMT models and to Dr. D.R. Larson, Dr. M.H. Sung, W.G. Mueller and Dr. F. Mueller for constructive feedback on the manuscript.

FUNDING

Intramural program of the National Institutes of Health (NIH), National Cancer Institute, Center for Cancer Research; Marie Curie international incoming fellowship [27432 to D.M., in part]. Funding for open access charge: NIH intramural program.

Conflict of interest statement. None declared.

REFERENCES

1. Phair,R.D. and Misteli,T. (2001) Kinetic modelling approaches to in vivo imaging. *Nat. Rev. Mol. Cell Biol.*, **2**, 898–907.
2. Elf,J., Li,G.-W. and Xie,X.S. (2007) Probing transcription factor dynamics at the single-molecule level in a living cell. *Science*, **316**, 1191–1194.
3. Hager,G.L., McNally,J.G. and Misteli,T. (2009) Transcription dynamics. *Mol. Cell*, **35**, 741–753.
4. Kang,M., Day,C.A., DiBenedetto,E. and Kenworthy,A.K. (2010) A quantitative approach to analyze binding diffusion kinetics by confocal FRAP. *Biophys. J.*, **99**, 2737–2747.
5. Phair,R.D. and Misteli,T. (2000) High mobility of proteins in the mammalian cell nucleus. *Nature*, **404**, 604–609.
6. Mueller,F., Wach,P. and McNally,J.G. (2008) Evidence for a common mode of transcription factor interaction with chromatin as revealed by improved quantitative fluorescence recovery after photobleaching. *Biophys. J.*, **94**, 3323–3339.
7. Yao,J., Munson,K.M., Webb,W.W. and Lis,J.T. (2006) Dynamics of heat shock factor association with native gene loci in living cells. *Nature*, **442**, 1050–1053.
8. Michelman-Ribeiro,A., Mazza,D., Rosales,T., Stasevich,T.J., Boukari,H., Rishi,V., Vinson,C., Knutson,J.R. and McNally,J.G. (2009) Direct measurement of association and dissociation rates of DNA binding in live cells by fluorescence correlation spectroscopy. *Biophys. J.*, **97**, 337–346.
9. Capoulade,J., Wachsmuth,M., Hufnagel,L. and Knop,M. (2011) Quantitative fluorescence imaging of protein diffusion and interaction in living cells. *Nat. Biotechnol.*, **29**, 835–839.
10. Grünwald,D., Spottke,B., Buschmann,V. and Kubitscheck,U. (2006) Intranuclear binding kinetics and mobility of single native U1 snRNP particles in living cells. *Mol. Biol. Cell*, **17**, 5017–5027.
11. Speil,J., Baumgart,E., Siebrasse,J.-P., Veith,R., Vinkemeier,U. and Kubitscheck,U. (2011) Activated STAT1 transcription factors conduct distinct saltatory movements in the cell nucleus. *Biophys. J.*, **101**, 2592–2600.
12. Hinow,P., Rogers,C.E., Barbieri,C.E., Pietenpol,J.A., Kenworthy,A.K. and DiBenedetto,E. (2006) The DNA binding activity of p53 displays reaction-diffusion kinetics. *Biophys. J.*, **91**, 330–342.
13. Phair,R.D., Scaffidi,P., Elbi,C., Vecerová,J., Dey,A., Ozato,K., Brown,D.T., Hager,G., Bustin,M. and Misteli,T. (2004) Global nature of dynamic protein-chromatin interactions in vivo: three-dimensional genome scanning and dynamic interaction networks of chromatin proteins. *Mol. Cell. Biol.*, **24**, 6393–6402.
14. Dundr,M., Hoffmann-Rohrer,U., Hu,Q., Grummt,I., Rothblum,L.I., Phair,R.D. and Misteli,T. (2002) A kinetic framework for a mammalian RNA polymerase in vivo. *Science*, **298**, 1623–1626.
15. Darzacq,X., Shav-Tal,Y., de Turris,V., Brody,Y., Shenoy,S.M., Phair,R.D. and Singer,R.H. (2007) In vivo dynamics of RNA polymerase II transcription. *Nat. Struct. Mol. Biol.*, **14**, 796–806.
16. Kimura,H., Sugaya,K. and Cook,P.R. (2002) The transcription cycle of RNA polymerase II in living cells. *J. Cell Biol.*, **159**, 777–782.
17. Maiuri,P., Knezevich,A., De Marco,A., Mazza,D., Kula,A., McNally,J.G. and Marcello,A. (2011) Fast transcription rates of RNA polymerase II in human cells. *EMBO Rep.*, **12**, 1280–1285.
18. Larson,D.R., Zenklusen,D., Wu,B., Chao,J.A. and Singer,R.H. (2011) Real-time observation of transcription initiation and elongation on an endogenous yeast gene. *Science*, **332**, 475–478.
19. Mueller,F., Mazza,D., Stasevich,T.J. and McNally,J.G. (2010) FRAP and kinetic modeling in the analysis of nuclear protein dynamics: what do we really know? *Curr. Opin. Cell Biol.*, **22**, 403–411.
20. Farla,P., Hersmus,R., Trapman,J. and Houtsmuller,A.B. (2005) Antiandrogens prevent stable DNA-binding of the androgen receptor. *J. Cell. Sci.*, **118**, 4187–4198.
21. Hendrix,J., Gijsbers,R., De Rijck,J., Voet,A., Hotta,J.-I., McNeely,M., Hofkens,J., Debyser,Z. and Engelborghs,Y. (2010) The transcriptional co-activator LEDGF/p75 displays a dynamic scan-and-lock mechanism for chromatin tethering. *Nucleic Acids Res.*, 10.1093/nar/gkq933.
22. Mikuni,S., Tamura,M. and Kinjo,M. (2007) Analysis of intranuclear binding process of glucocorticoid receptor using fluorescence correlation spectroscopy. *FEBS Lett.*, **581**, 389–393.
23. Babcock,H.P., Chen,C. and Zhuang,X. (2004) Using single-particle tracking to study nuclear trafficking of viral genes. *Biophys. J.*, **87**, 2749–2758.
24. Tokunaga,M., Imamoto,N. and Sakata-Sogawa,K. (2008) Highly inclined thin illumination enables clear single-molecule imaging in cells. *Nat. Methods*, **5**, 159–161.

25. Weigel,A.V., Simon,B., Tamkun,M.M. and Krapf,D. (2011) Ergodic and nonergodic processes coexist in the plasma membrane as observed by single-molecule tracking. *Proc. Natl Acad. Sci. USA*, **108**, 6438–6443.
26. Speil,J. and Kubitscheck,U. (2010) Single ovalbumin molecules exploring nucleoplasm and nucleoli of living cell nuclei. *Biochim. Biophys. Acta*, **1803**, 396–404.
27. Bancaud,A., Huet,S., Daigle,N., Mozziconacci,J., Beaudouin,J. and Ellenberg,J. (2009) Molecular crowding affects diffusion and binding of nuclear proteins in heterochromatin and reveals the fractal organization of chromatin. *EMBO J.*, **28**, 3785–3798.
28. Stasevich,T.J., Mueller,F., Michelman-Ribeiro,A., Rosales,T., Knutson,J.R. and McNally,J.G. (2010) Cross-validating FRAP and FCS to quantify the impact of photobleaching on in vivo binding estimates. *Biophys. J.*, **99**, 3093–3101.
29. Schröder,J., Benink,H., Dyba,M. and Los,G.V. (2009) In vivo labeling method using a genetic construct for nanoscale resolution microscopy. *Biophys. J.*, **96**, L01–03.
30. Selvin,P.R. and Ha,T. (2007) *Single-Molecule Techniques: A Laboratory Manual*, 1st edn. Cold Spring Harbor Laboratory Press, Cold Spring Harbor, NY.
31. Kimura,H. and Cook,P.R. (2001) Kinetics of core histones in living human cells: little exchange of H3 and H4 and some rapid exchange of H2B. *J. Cell Biol.*, **153**, 1341–1353.
32. Marshall,W.F., Straight,A., Marko,J.F., Swedlow,J., Dernburg,A., Belmont,A., Murray,A.W., Agard,D.A. and Sedat,J.W. (1997) Interphase chromosomes undergo constrained diffusional motion in living cells. *Curr. Biol.*, **7**, 930–939.
33. Neumann,F.R., Dion,V., Gehlen,L.R., Tsai-Pflugfelder,M., Schmid,R., Taddei,A. and Gasser,S.M. (2012) Targeted INO80 enhances subnuclear chromatin movement and ectopic homologous recombination. *Genes Dev.*, **26**, 369–383.
34. Veith,R., Sorkalla,T., Baumgart,E., Anzt,J., Häberlein,H., Tyagi,S., Siebrasse,J.P. and Kubitscheck,U. (2010) Balbiani ring mRNPs diffuse through and bind to clusters of large intranuclear molecular structures. *Biophys. J.*, **99**, 2676–2685.
35. Sprague,B.L., Pego,R.L., Stavreva,D.A. and McNally,J.G. (2004) Analysis of binding reactions by fluorescence recovery after photobleaching. *Biophys. J.*, **86**, 3473–3495.
36. Yechiel,E. and Edidin,M. (1987) Micrometer-scale domains in fibroblast plasma membranes. *J. Cell Biol.*, **105**, 755–760.
37. Kaeser,M.D. and Iggo,R.D. (2002) Chromatin immunoprecipitation analysis fails to support the latency model for regulation of p53 DNA binding activity in vivo. *Proc. Natl Acad. Sci. USA*, **99**, 95–100.
38. Tafvizi,A., Huang,F., Fersht,A.R., Mirny,L.A. and van Oijen,A.M. (2011) A single-molecule characterization of p53 search on DNA. *Proc. Natl Acad. Sci. USA*, **108**, 563–568.
39. Berkovich,R., Wolfenson,H., Eisenberg,S., Ehrlich,M., Weiss,M., Klafter,J., Henis,Y.I. and Urbakh,M. (2011) Accurate quantification of diffusion and binding kinetics of non-integral membrane proteins by FRAP. *Traffic*, **12**, 1648–1657.
40. Hamard,P.-J., Lukin,D.J. and Manfredi,J.J. (2012) p53 basic C-terminus regulates p53 functions through DNA binding modulation of a subset of target genes. *J. Biol. Chem.*, **287**, 22397–22407.
41. Kim,H., Kim,K., Choi,J., Heo,K., Baek,H.J., Roeder,R.G. and An,W. (2012) p53 requires an intact C-terminal domain for DNA binding and transactivation. *J. Mol. Biol.*, **415**, 843–854.
42. McNally,J.G., Müller,W.G., Walker,D., Wolford,R. and Hager,G.L. (2000) The glucocorticoid receptor: rapid exchange with regulatory sites in living cells. *Science*, **287**, 1262–1265.
43. Rayasam,G.V., Elbi,C., Walker,D.A., Wolford,R., Fletcher,T.M., Edwards,D.P. and Hager,G.L. (2005) Ligand-specific dynamics of the progesterone receptor in living cells and during chromatin remodeling in vitro. *Mol. Cell. Biol.*, **25**, 2406–2418.
44. Bosisio,D., Marazzi,I., Agresti,A., Shimizu,N., Bianchi,M.E. and Natoli,G. (2006) A hyper-dynamic equilibrium between promoter-bound and nucleoplasmic dimers controls NF-kappaB-dependent gene activity. *EMBO J.*, **25**, 798–810.
45. Beck,M., Schmidt,A., Malmstroem,J., Claassen,M., Ori,A., Szymborska,A., Herzog,F., Rinner,O., Ellenberg,J. and Aebersold,R. (2011) The quantitative proteome of a human cell line. *Mol. Syst. Biol.*, **7**, 549.
46. Lahav,G., Rosenfeld,N., Sigal,A., Geva-Zatorsky,N., Levine,A.J., Elowitz,M.B. and Alon,U. (2004) Dynamics of the p53-Mdm2 feedback loop in individual cells. *Nat. Genet.*, **36**, 147–150.
47. Smeenk,L., van Heeringen,S.J., Koeppel,M., Gilbert,B., Janssen-Megens,E., Stunnenberg,H.G. and Lohrum,M. (2011) Role of p53 serine 46 in p53 target gene regulation. *PLoS ONE*, **6**, e17574.
48. Los,G.V. and Wood,K. (2007) The HaloTag: a novel technology for cell imaging and protein analysis. *Methods Mol. Biol.*, **356**, 195–208.
49. Rosenke,K., Samuel,M.A., McDowell,E.T., Toerne,M.A. and Fortunato,E.A. (2006) An intact sequence-specific DNA-binding domain is required for human cytomegalovirus-mediated sequestration of p53 and may promote in vivo binding to the viral genome during infection. *Virology*, **348**, 19–34.
50. Crank,J. (1980) *The Mathematics of Diffusion*, 2nd edn. Oxford University Press, Oxford, UK.
51. Matsuoka,S., Shibata,T. and Ueda,M. (2009) Statistical analysis of lateral diffusion and multistate kinetics in single-molecule imaging. *Biophys. J.*, **97**, 1115–1124.
52. Crocker,J.C. and Grier,D.G. (1996) Methods of digital video microscopy for colloidal studies. *J. Coll. Int. Sci.*, **179**, 298–310.
53. Yeung,C., Shtrahman,M. and Wu,X. (2007) Stick-and-diffuse and caged diffusion: a comparison of two models of synaptic vesicle dynamics. *Biophys. J.*, **92**, 2271–2280.
54. Kues,T. and Kubitscheck,U. (2002) Single molecule motion perpendicular to the focal plane of a microscope: application to splicing factor dynamics within the cell nucleus. *Single Mol.*, **3**, 218–224.